International Journal of Engineering & Applied Sciences (IJEAS)
Vol.7, Issue 1(2015)68-85

SHEAR AND VOLUMETRIC LOCKING EFFECT ON THE PERFORMANCE OF HARMONIC SOLID RING FINITE ELEMENTS

Ali İ. Karakaş1 [a*] *and Ayse T. Daloğlu2*[b]

[a,b] *Karadeniz Technical University, Department of Civil Engineering, 61080 Trabzon, Turkey*
[*]*E-mail address: aliihsanka@yahoo.com*

Received date: February 2015
Accepted date: February 2015

Abstract

Harmonic solid ring finite elements are commonly used in the analysis of axisymmetric structures subjected to non-axisymmetric as well as axisymmetric loadings. Depending on the material and/or geometrical properties of axisymmetric problems the finite element analysis may produce erroneous solutions due to approximations assumed in the formulation. Volumetric and shear locking are the some troublesome behaviors of some finite elements. In this study, finite element formulations of 4-noded (Ring4) and 9-noded (Ring9) ring elements are developed considering constant and linear shear locking effect for the element types, respectively, by incorporating selectively reduced integration technique. A computer program is coded in Matlab for the purpose and the performances of both elements are explored in terms of locking issue as well as accuracy. For this purpose several axisymmetric problems are solved such as hollow thick cylinder and circular plate problems. Numerical results indicate that while Ring9 does not suffer from volumetric locking for high values of Poisson's ratios Ring4 suffers. Besides, while Ring4 with full integration displays shear locking effects Ring4 with selectively reduced integration eliminates the locking. The finite element formulations are explained in detail and the results of numerical examples are presented comparatively in graphical and tabular formats.

Keywords: shear and volumetric locking, harmonic solid ring element, selectively reduced integration

1. Introduction

Finite elements are versatile and most commonly used numerical method among researchers and practitioners to solve complex problems in engineering and science. Sometimes unpredicted behaviors under certain conditions can be experienced due to the approximations made in the finite element formulations. Assumptions made in the displacement functions to represent real behavior of the system and applications of programming friendly numerical integration techniques instead of continuous integration may end up with some erratic manners in the result. For instance, shear and volumetric locking are the most important problematic behaviors that can occur in finite element formulations. The locking phenomenon is characterized by a severe underestimation of the displacements, i.e. the structure is too stiff. The word "locking" means that the structure "locks" itself against deformations. Also, locking means the effect of a reduced rate of convergence for coarse meshes in dependence of a critical parameter such as thickness [1].When nearly incompressible material or thin shell applications are described using the standard finite elements some numerical problems or erroneous solutions may arise due to locking effects [2-4]. In order to alleviate locking problems several solutions are proposed in the literature [5-9]. Reduced and selectively reduced integration techniques, mixed formulation technique and enhanced strain method are the most common solution procedures described in literature. In this study the finite element

formulations of 4-noded (Ring4) and 9-noded (Ring9) harmonic solid ring with selectively reduced integration techniques are presented in general terms to solve locking problems in axisymmetric structures. In selectively reduced integration procedure the shear strain terms are only integrated using reduced Gauss points. In other words, in the stiffness formulations the normal strain terms are integrated using required number of Gauss points for the exact evaluation of integrals whereas the shear strain terms are integrated using lesser number of Gauss points. Additionally, the performance of the developed quadrilateral harmonic solid ring finite elements is investigated as far as volumetric and shear locking problems are considered for axisymmetric thin or thick solid structures. For this purposes several numerical studies are performed using the finite element program coded in Matlab. A thick cylinder is studied to mainly focus on volumetric locking by changing Poisson's ratio, and shear locking is explained considering circular plate subjected to pure bending with varying thicknesses.

2. Harmonic Finite Element Model

For harmonic model in linear elastic analysis, it is possible to demonstrate both the loads and the displacement as Fourier series expansions in terms of circumferential coordinate θ [10].

$$\{u(r,\theta,z)\} = \begin{Bmatrix} u_r \\ u_\theta \\ u_z \end{Bmatrix} = \begin{Bmatrix} \bar{u}_r + \bar{\bar{u}}_r \\ \bar{u}_\theta + \bar{\bar{u}}_\theta \\ \bar{u}_z + \bar{\bar{u}}_z \end{Bmatrix} = \begin{Bmatrix} \sum_{m=0}^{\infty} \bar{u}_{rm} \cos m\theta + \sum_{m=0}^{\infty} \bar{\bar{u}}_{rm} \sin m\theta \\ \sum_{m=0}^{\infty} \bar{u}_{\theta m} \sin m\theta - \sum_{m=0}^{\infty} \bar{\bar{u}}_{\theta m} \cos m\theta \\ \sum_{m=0}^{\infty} \bar{u}_{zm} \cos m\theta + \sum_{m=0}^{\infty} \bar{\bar{u}}_{zm} \sin m\theta \end{Bmatrix} \tag{1}$$

where m is the circumferential mode (harmonic) number and symbols u_r, u_θ and u_z indicate the radial, circumferential and axial displacement components, respectively, see Fig. 1. All barred quantities in Eq.(1) are amplitudes approximated using the finite element method, which are functions of r, z but not of θ. This produces a harmonic finite element in the (r, z) plane. Single and double barred amplitudes represent symmetric ($f(\theta) = f(-\theta)$) and anti-symmetric ($f(\theta) = -f(-\theta)$) displacement terms, respectively. The amplitudes of the displacement components in Eq. (1) can be interpolated from nodal amplitudes using the shape functions. Fig. 1 shows the shape and node numbering of the ring elements as well as coordinatesystems.

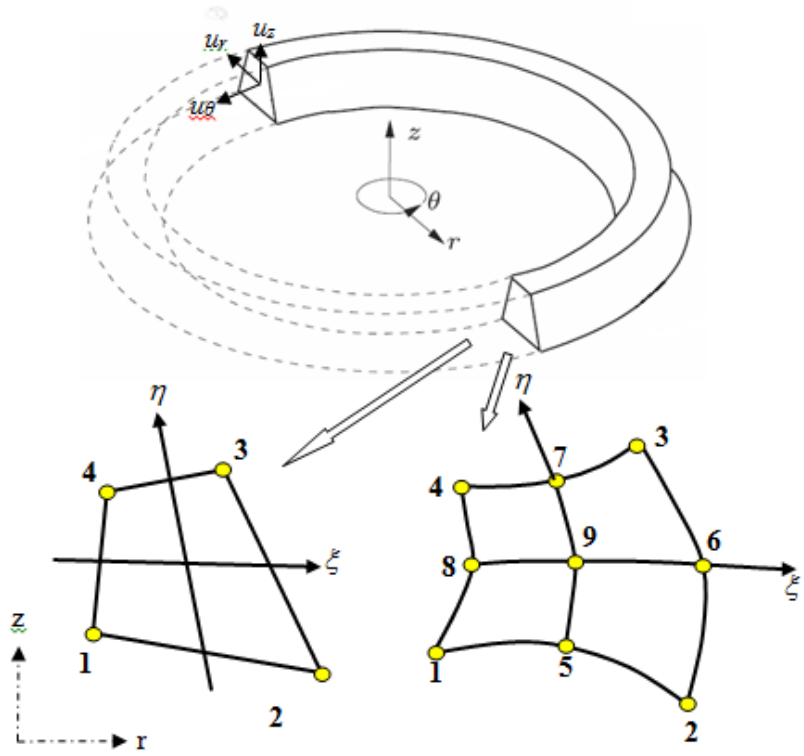

Figure1: Displacement components, nodal numbering and cross sections of Ring4 and Ring9 elements.

In this study the formulation of symmetric part of the harmonic ring finite element is presented for the simplicity and a detailed explanation and anti-symmetric formulation can be found in [11]. The vector of displacement field within the element can be described such that subscript *im* specifies that amplitude refers to node *i* and harmonic *m* [12].

$$\{\bar{u}\} = \begin{Bmatrix} \bar{u}_r(r,\theta,z) \\ \bar{u}_\theta(r,\theta,z) \\ \bar{u}_z(r,\theta,z) \end{Bmatrix} = \sum_{m=0}^{\infty} \left(\left[\overline{g_{\theta m}} \right]_u [N] \{\bar{d}_m\} \right) \tag{2}$$

where $\{\bar{d}\}_m$ is the nodal displacement vector for the Fourier term (mode) *m* and $[N]$ is the shape functions matrix, which are defined as

$$\{\bar{d}\}_m = \left[\{\bar{u}_{1m}\}^T \quad \{\bar{u}_{2m}\}^T \quad .... \quad \{\bar{u}_{bm}\}^T \right]^T \tag{2}$$

$$[N] = \left[[N]_1 \quad [N]_2 \quad ..... \quad [N]_b \right] \tag{3}$$

where

$$[N]_i = \begin{bmatrix} N_i & 0 & 0 \\ 0 & N_i & 0 \\ 0 & 0 & N_i \end{bmatrix} \tag{4}$$

where *b*=4 for bilinear (Ring4) and *b*=9 for biquadratic (Ring9) quadrilateral elements. The shape functions at each node *i* for both quadrilateral elements are given in [13, 14].

Also, the matrices of harmonic functions for harmonic m are

$$\left[\overline{g_{\theta m}}\right]_u = \begin{bmatrix} \cos m\theta & 0 & 0 \\ 0 & \sin m\theta & 0 \\ 0 & 0 & \cos m\theta \end{bmatrix} \tag{5}$$

Strains and stresses in an element can also be stated in terms of the Fourier series. For a Fourier term m, the strain vector in cylindrical coordinates can be written as:

$$\left\{\overline{\varepsilon}\right\}_m = \begin{Bmatrix} \dfrac{\partial u_{rm}}{\partial r} \\ \dfrac{1}{r}(u_{rm} + \dfrac{\partial u_{\theta m}}{\partial \theta}) \\ \dfrac{\partial u_{zm}}{\partial z} \\ \dfrac{\partial u_{zm}}{\partial r} + \dfrac{\partial u_{rm}}{\partial z} \\ \dfrac{1}{r}\dfrac{\partial u_{rm}}{\partial \theta} + \dfrac{\partial u_{\theta m}}{\partial r} - \dfrac{u_{\theta m}}{r} \\ \dfrac{\partial u_{\theta m}}{\partial z} + \dfrac{1}{r}\dfrac{\partial u_{zm}}{\partial \theta} \end{Bmatrix} = \left[\overline{B}_m\right]\left\{\overline{d}_m\right\} \tag{6}$$

The strain displacement matrices can be stated as follows for harmonic m:

$$\left[\overline{B}\right]_m = \left[\overline{g_{\theta m}}\right][B]_m = \left[\overline{g_{\theta m}}\right]\begin{bmatrix} [B_m]_\varepsilon \\ [B_m]_\gamma \end{bmatrix} = \left[\overline{g_{\theta m}}\right]\begin{bmatrix} [B]_{11m} & [B]_{12m} & .... & [B]_{1bm} \\ [B]_{21m} & [B]_{22m} & .... & [B]_{2bm} \end{bmatrix} \tag{7}$$

where $\left[\overline{B}_m\right]$ is the matrix which relates the symmetric nodal displacement amplitudes with corresponding strains and the matrix $\left[\overline{g_{\theta m}}\right]$ of the harmonic functions for the harmonic m is:

$$\left[\overline{g_{\theta m}}\right] = \begin{bmatrix} \left[\overline{g_{\theta m}}\right]_\varepsilon & 0 \\ 0 & \left[\overline{g_{\theta m}}\right]_\gamma \end{bmatrix} \tag{8}$$

where $\left[\overline{g_{\theta m}}\right]_\varepsilon = \cos m\theta \begin{bmatrix} 1 & 0 & 0 \\ 0 & 1 & 0 \\ 0 & 0 & 1 \end{bmatrix}$ and $\left[\overline{g_{\theta m}}\right]_\gamma = \begin{bmatrix} \cos m\theta & 0 & 0 \\ 0 & \sin m\theta & 0 \\ 0 & 0 & \sin m\theta \end{bmatrix}$ (9)

and for the i^{th} node, the submatrices are given as:

$$[B]_{1im} = \begin{bmatrix} N_{i,r} & 0 & 0 \\ \dfrac{N_i}{r} & \dfrac{mN_i}{r} & 0 \\ 0 & 0 & N_{i,z} \end{bmatrix} \tag{10}$$

$$[B]_{2im} = \begin{bmatrix} N_{i,z} & 0 & N_{i,r} \\ -\dfrac{mN_i}{r} & (N_{i,r} - \dfrac{N_i}{r}) & 0 \\ 0 & N_{j,z} & -\dfrac{mN_i}{r} \end{bmatrix} \tag{11}$$

The stress vector for the m^{th} harmonic in the cylindrical coordinate system related to the strain vector through the constitutive equations is given for an isotropic material as follows [14]

$$\{\bar{\sigma}\}_m = [D]\{\bar{\varepsilon}\}_m \tag{12}$$

in which $[D]$ is the material property matrix for isotropic material given by the following equation where E modulus of elasticity and v is Poisson's ratio

$$[D] = \begin{bmatrix} [E_\varepsilon] & 0 \\ 0 & [E_\gamma] \end{bmatrix} \tag{13}$$

where $$[E_\varepsilon] = \frac{E}{(1+v)(1-2v)} \begin{bmatrix} 1-v & v & v \\ v & 1-v & v \\ v & v & 1-v \end{bmatrix} \quad \text{and} \quad [E_\gamma] = \frac{E}{2(1+v)} \tag{14}$$

2. Element Matrices

2.1. The element stiffness matrix

The stiffness matrix of a linear system is calculated from the derivation of the strain energy of an axisymmetric solid ring element [15]. The element strain energy is given as:

$$U_e = \frac{1}{2}\int \{\varepsilon\}^T \{\sigma\} dV = \frac{1}{2}\{d\}^T [k]\{d\} \tag{15}$$

Substituting Eqs. (6) and (12) into Eq. (15) for single barred terms the stiffness matrix for symmetric terms in Fourier series expansion is obtained as:

$$\left[\bar{k}_m\right] = \iint [B_m]^T \left(\int_0^{2\pi} \begin{bmatrix} \left[\overline{g_{\theta m}}\right]_\varepsilon^T [E_\varepsilon] \left[\overline{g_{\theta m}}\right]_\varepsilon & 0 \\ 0 & \left[\overline{g_{\theta m}}\right]_\gamma^T [E_\gamma] \left[\overline{g_{\theta m}}\right]_\gamma \end{bmatrix} d\theta \right) [B_m] r dr dz \tag{16}$$

It can be observed that each term in the products of $\left[\overline{g_{\theta m}}\right]_{\varepsilon}^{T}\left[E_{\varepsilon}\right]\left[\overline{g_{\theta m}}\right]_{\varepsilon}$, $\left[\overline{g_{\theta m}}\right]_{\gamma}^{T}\left[E_{\gamma}\right]\left[\overline{g_{\theta m}}\right]_{\gamma}$ will be a function of (E, v) multiplied by either $\cos^2 m\theta$ or $\sin^2 m\theta$. Thus, integration over the circumferential direction θ can be carried out explicitly. The stiffness matrix of a quadrilateral ring element can be numerically integrated by Gauss quadrature rule which is very suitable for finite element applications. If both the bending (ε) and shear terms (γ) in the stiffness matrix are integrated using *p1= p2* Gauss points then it is called Full Integration (FI). And it is called Selectively Reduced Integration (SRI) technique in which the bending terms are integrated using (*p1*)-point Gauss quadrature rule and the shear terms are integrated using (*p*2)-point Gauss quadrature rule. By taking explicit integrations and using numerical integration the stiffness matrices for symmetric terms are calculated from the following expressions:

$$\left[\overline{k}_0\right] = 2\pi \left(\begin{array}{l} \sum_{k=1}^{p1}\sum_{l=1}^{p1} w_k w_l \left[B_0\right]_{\varepsilon}^{T}(\xi_k,\eta_l)\left[\overline{E}_{\varepsilon o}\right]\left[B_0\right]_{\varepsilon}(\xi_k,\eta_l) r(\xi_k,\eta_l) J(\xi_k,\eta_l) \\ +\sum_{k=1}^{p2}\sum_{l=1}^{p2} w_k w_l \left[B_0\right]_{\gamma}^{T}(\xi_k,\eta_l)\left[\overline{E}_{\gamma 0}\right]\left[B_0\right]_{\gamma}(\xi_k,\eta_l) r(\xi_k,\eta_l) J(\xi_k,\eta_l) \end{array} \right) \tag{17}$$

for m >0

$$\left[\overline{k}_m\right] = \pi \left(\begin{array}{l} \sum_{k=1}^{p1}\sum_{l=1}^{p1} w_k w_l \left[B_m\right]_{\varepsilon}^{T}(\xi_k,\eta_l)\left[E_{\varepsilon}\right]\left[B_m\right]_{\varepsilon}(\xi_k,\eta_l) r(\xi_k,\eta_l) J(\xi_k,\eta_l) \\ +\sum_{k=1}^{p2}\sum_{l=1}^{p2} w_k w_l \left[B_m\right]_{\gamma}^{T}(\xi_k,\eta_l)\left[E_{\gamma}\right]\left[B_m\right]_{\gamma}(\xi_k,\eta_l) r(\xi_k,\eta_l) J(\xi_k,\eta_l) \end{array} \right) \tag{18}$$

where ξ_k and η_l are the Gauss points abcissae whereas w_k and w_l are the corresponding integration weights. Also $\left[B_m\right]_{\varepsilon}(\xi_k,\eta_l)$ and $\left[B_m\right]_{\gamma}(\xi_k,\eta_l)$ mean that these matrices are evaluated at Gauss points; likewise for $r(\xi_k,\eta_l)$, the radius of Gauss point and $J(\xi_k,\eta_l)$, Jacobian determinant that transforms the element from global coordinates (*r, z*) to the natural coordinates (ξ, η). The number of Gauss points used for full and selectively reduced integration are given in Table 1.

Table 1. Gauss point numbers

Element Type	Full integration(FI)		Selectively Reduced Integration(SRI)	
	*p1*x*p1*	*p2*x*p2*	*p1*x*p1*	*p2*x*p2*
Ring4	2x2	2x2	2x2	1x1
Ring9	3x3	3x3	3x3	2x2

2.2. The element force vectors

The consistent force vectors are calculated from the derivation of the work done by the applied loads. Using *p*-point two dimensional Gauss quadrature rule we have the following expressions for the consistent body force vectors for symmetric Fourier harmonics as:

for m=0

$$\{\overline{f}_{b0}\} = 2\pi \sum_{k=1}^{p}\sum_{l=1}^{p} w_k w_l \left[N\right]^T (\xi_k,\eta_l) \begin{bmatrix} 1 & 0 & 0 \\ 0 & 0 & 0 \\ 0 & 0 & 1 \end{bmatrix} \{\overline{q}_{b0}\} r(\xi_k,\eta_l) J(\xi_k,\eta_l) \tag{19}$$

for m>0

$$\{\overline{f}_{bm}\} = \pi \sum_{k=1}^{p}\sum_{l=1}^{p} w_k w_l \left[N\right]^T (\xi_k,\eta_l) \{\overline{q}_{bm}\} r(\xi_k,\eta_l) J(\xi_k,\eta_l) \tag{20}$$

where $\left\{\overline{q}_{bm}\right\}$ is the body load amplitude vector for the Fourier term *m* of symmetric loads. Also, unidimensional numerical integration can be applied for the consistent force vector associated with surface traction. Then we have the following expressions in which J_Γ is the associated arc length Jacobian.

for m=0

$$\{\overline{f}_{s0}\} = 2\pi \sum_{k=1}^{p} w_k \left[N\right]_s^T (\xi_k) \begin{bmatrix} 1 & 0 & 0 \\ 0 & 0 & 0 \\ 0 & 0 & 1 \end{bmatrix} \{q_{s0}\} r(\xi_k) J_\Gamma(\xi_k) \tag{21}$$

for m>0

$$\{\overline{f}_{sm}\} = \pi \sum_{k=1}^{p} w_k \left[N\right]_s^T (\xi_k) \{\overline{q}_{sm}\} r(\xi_k) J_\Gamma(\xi_k) \tag{22}$$

where $\left[N\right]_s$ is the values of $\left[N\right]$ at locations of surface load vectors and $\left\{\overline{q}_{sm}\right\}$ is the surface load amplitude vector for the Fourier term *m*.

3. Solution Procedure

In this study we are concerned with the solution of the simultaneous equations that arise in the static analysis of axisymmetric structures using finite element method. The matrix equation for static problems is given by

$$\left[\overline{K}_m\right]\left\{\overline{U}_m\right\} = \left\{\overline{F}_m\right\} \tag{23}$$

where $\left[\overline{K}_m\right]$ is the system stiffness matrix, $\left\{\overline{U}_m\right\}$ is the system nodal displacement amplitude vector, and $\left\{\overline{F}_m\right\}$ is the system nodal force amplitude vector for symmetric harmonic mode *m* and single barred terms in Fourier series expansion. Solution of the equation is obtained by the Gauss elimination procedure.

4. Numerical Examples

The static deformations of a hollow cylinder under various loadings, an internally pressurized thick cylinder and a circular plate bending problem are investigated for volumetric and shear locking behaviors using Ring4 and Ring9 harmonic solid finite elements. Full and selectively reduced integration techniques are applied to get rid of locking effect on both the elements and comparisons are made.

4.1. Hollow Cylinder Under Various Loadings

A hollow cylinder with length L=0.6m, inner radius a=0.05m and outer radius b=0.06m with modulus of elasticity E=2x10^{11}Pa and Poisson's ratio v=0.3 is considered as the first example. The cylinder is investigated under three different loading cases which are axial load, torque and lateral point load. The magnitude of the loads are F_z=8x10^{3}N, T_z=4.4x10^{3}N and P=1x10^{3}N, respectively. The boundary condition of the cylinder is completely fixed at one end and free at the other end. The loads are applied at the top of the hollow cylinder. The analytical solutions of this problem can be obtained from mechanic of materials for axial elongation, rotation and tip deflection [16].

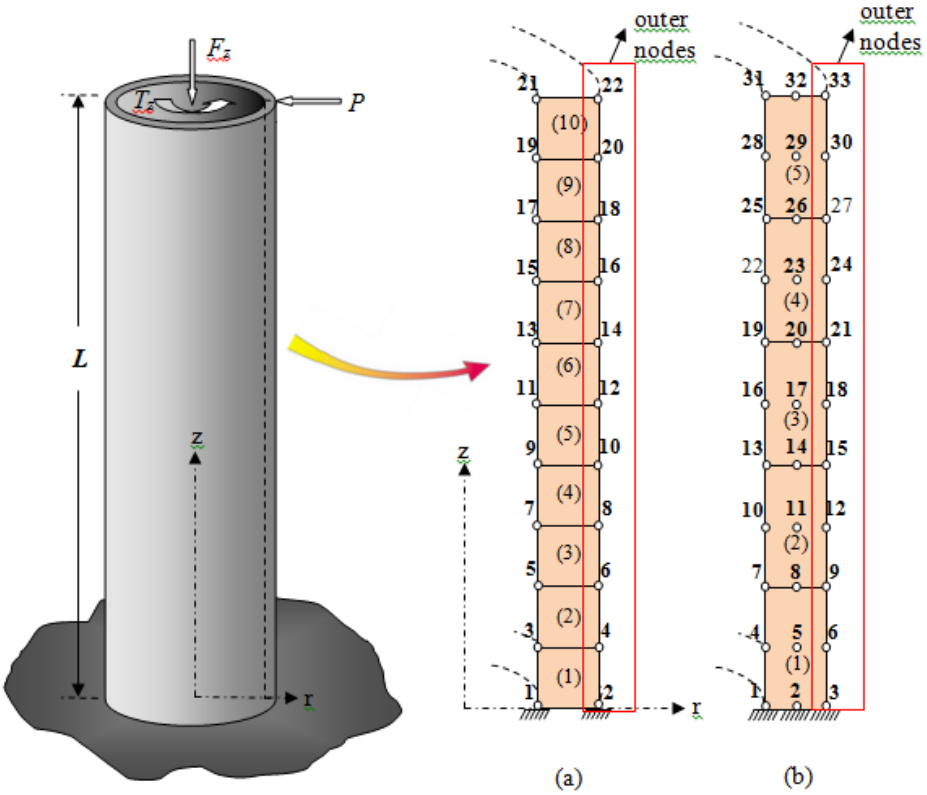

Figure 2: FEM discretization for the hollow cylinder (a) 10-element Ring4 discretization (b) 5-element Ring9 discretization

Finite element discretizations of the cylinder are shown in Fig.2. 10 Ring4 and 5 Ring9 elements are used in the static deformation analysis under various loadings. The analytical results are compared with the ones obtained finite element method using Ring4 and Ring9 elements and given in Table 2. All relative errors are measured with respect to the analytical method. Numbers in brackets indicate the number of finite elements used.

Table 1. Cylinder deformations under various loadings

Deformation	Method			Relative error	
	Ring4 (10)	Ring9 (5)	Analytical	Ring4	Ring9
Elongation(m)	$6.870\text{x}10^{-6}$	$6.882\text{x}10^{-6}$	$6.945\text{x}10^{-6}$	1.1%	0.8%
Rotation(rad)	$3.255\text{x}10^{-3}$	$3.255\text{x}10^{-3}$	$3.256\text{x}10^{-3}$	0.03%	0.03%
Tip deflection(m)	$6.597\text{x}10^{-5}$	$6.835\text{x}10^{-5}$	$6.831\text{x}10^{-5}$	3.4%	0.06%

Considering the relative errors it can be said that the results obtained using both the ring elements agree well with the analytical solutions. It seems from Table 2 that Ring9 gives better results when relative errors are considered due to quadratic shape functions used. Also, it should be noted that mesh refinement can decrease the relative errors. Finally it can be concluded that both elements produces accurate results and the program coded for the study is verified with exact solutions. .

4.2. Internally Pressurized Thick Cylinder

A cylindrical hollow tube of inner radius a=160mm and outer radius b=320 mm subjected to internal pressure P=150 MPa as shown Fig. 3 is analyzed next. The problem can be considered as a plane strain state since the tube extends indefinitely along the z direction. The material is isotropic with elastic modulus E=$2\text{x}10^5$ MPa and Poisson's ratio v=*0.2*. A slice of thickness d is extracted and finite element discretizations are shown in Fig. 3(a, b) using four Ring4 and two Ring9 elements along the radial direction r and one along the axial direction z. The axial element number is assumed to be one because the solution only depends on r. The nodes move in radial direction only and the support conditions are given in Fig.3(a, b).

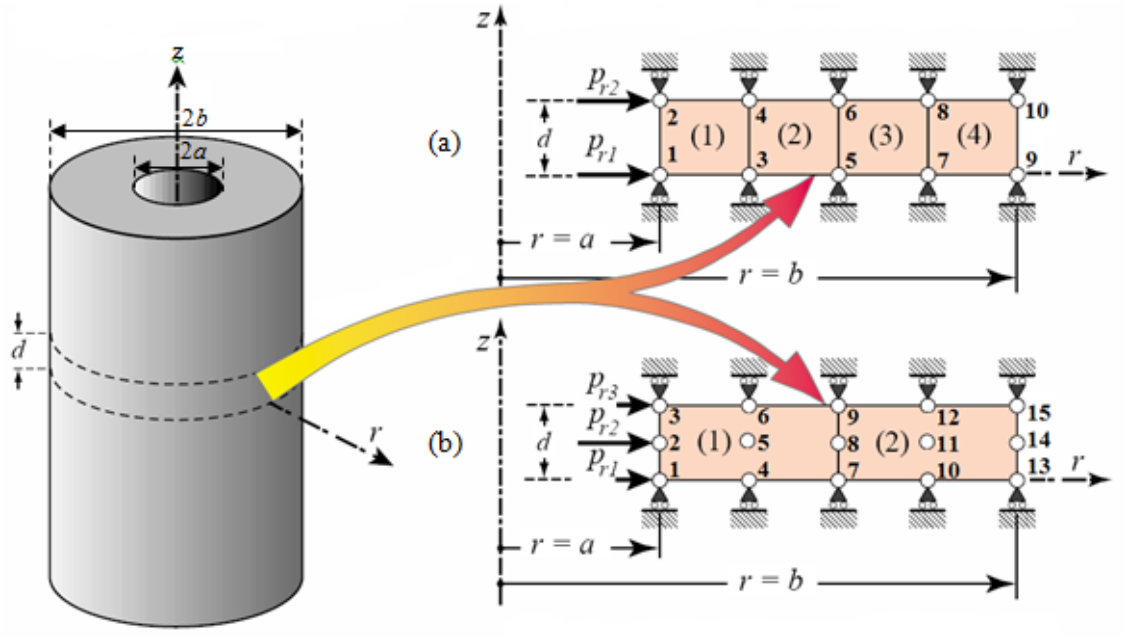

Figure 3: Two example FEM discretization for the pressurized thick cylinder (a) 4- element Ring4 discretization of a slice (b) 2-element Ring9 discretization of a slice

The exact stress distributions across the wall for a condition of plane strain in the z direction are obtained in [16]. The pressure lumping to the nodes on the inner radius r=a depends on the type of the element such as P_{r1}=P_{r2} for Ring4 and P_{r2}=$4P_{r2}$=$4P_{r3}$ for Ring9. The radial stresses σ_r and hoop stresses or circumferential stresses σ_θ are graphically compared over the

wall $a \leq r \leq b$ with the exact solutions in Fig.4 for various Poisson's ratios. If the Poisson ratio is increased over zero, Ring4 results gradually lose accuracy if the number of elements are kept as 16 as shown in Fig. 4(a, b). It can be shown that when the material gets closer to the limit state of Poisson's ratio for incompressibility the deterioration of the solution obtained speeds up. This phenomenon is known as volumetric locking in literature. Significant deficiencies can be observed. Also it should be noted that the volumetric locking is of a problem in such case that the plane strain condition does not allow the longitudinal expansion and contraction [1]. All stress components extremely oscillate as coming closer to the inner boundary and the values taken are meaningless. Besides a smaller stress oscillation can be observed at the outer boundary. For example, the radial stress is calculated as 48 MPa instead of -150 MPa at $r=a$ for $\nu = 0.485$. Modeling the same problem by using Ring9 makes a big difference. For an 8-element mesh in radial direction the radial hoop stresses are graphically compared over $a \leq r \leq b$ with the exact solution in Fig. 4(c, d). As can be seen volumetric locking or oscillations are not observed, and the stresses are well predicted everywhere. The agreement with the exact solution is excellent with Ring9 elements.

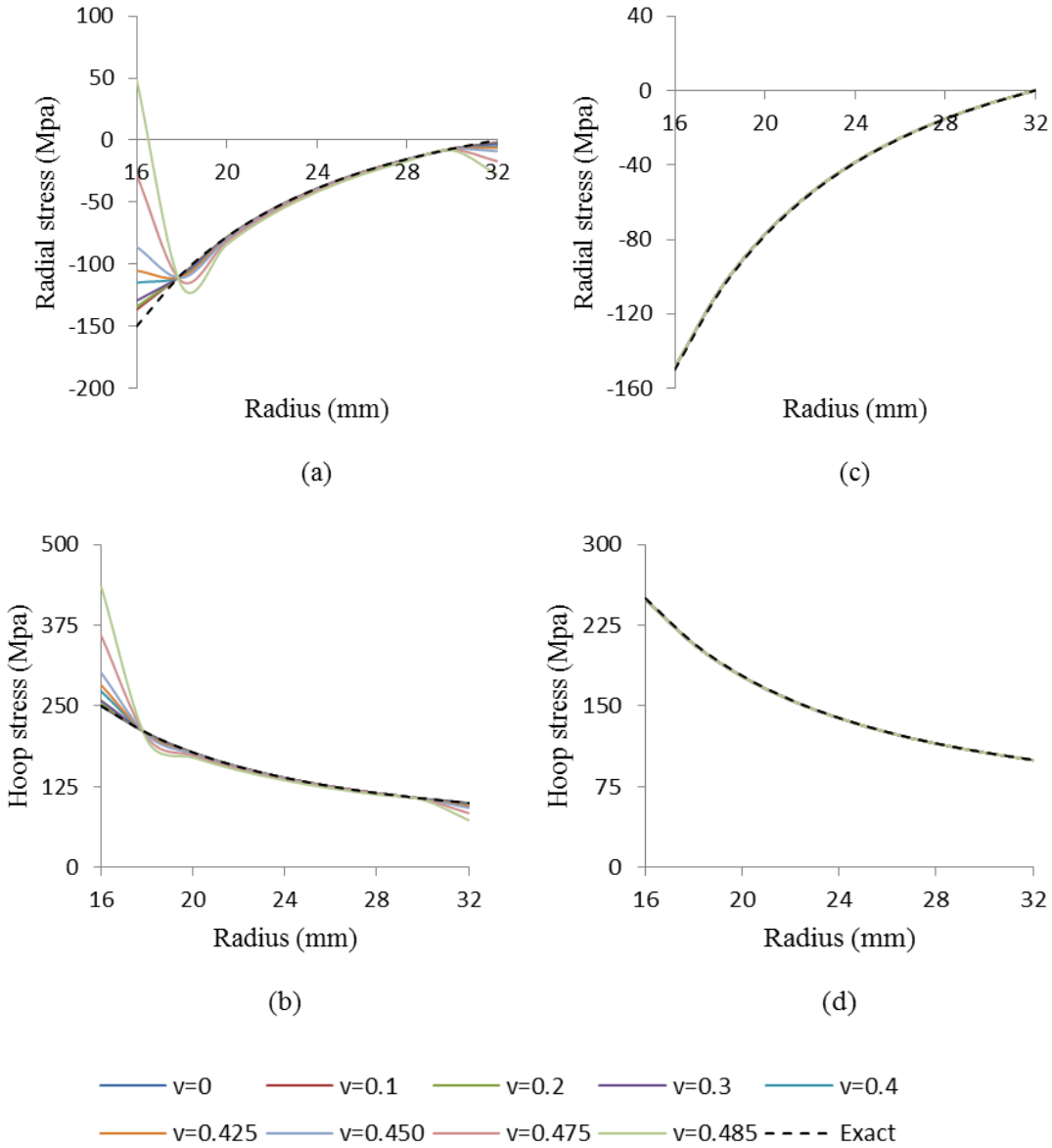

Figure 4: Computed versus exact (a) radial stresses with Ring4 (b) hoop stresses with Ring4 (c) radial stresses with Ring9 (d) hoop stresses with Ring9 for various values of Poisson's ratio

4.3. Circular Plate Bending

The last problem is a simply supported circular plate bending by a point load and uniformly distributed load as shown in Fig. 5(a). The plate has radius of R=10m and thickness of H=1m. The point load of magnitude P=500 kN acts downward at the plate center and uniformly distributed surface pressure of magnitude P_o=5 kN/m^2 acts downward over the whole top surface of the plate. The material is isotropic with elasticity modulus of E=30000 MPa and Poisson's ratio of v=0.2. Two FEM discretizations are pictured in Fig. 5(b, c). For Ring4 element 4x2, 8x2 and 16x2 discretizations are used, whereas for Ring9 the meshes are 2x1, 4x1 and 8x1 in radial and axial directions, respectively. Nodes are allowed to move in the z direction except those on the edge at r=R. The nodes at r=0 are constrained against radial deflection due to axial symmetry. The resulting support conditions are shown in Fig. 5(b, c). The central point load appropriately lumped to the nodes on the z axis.

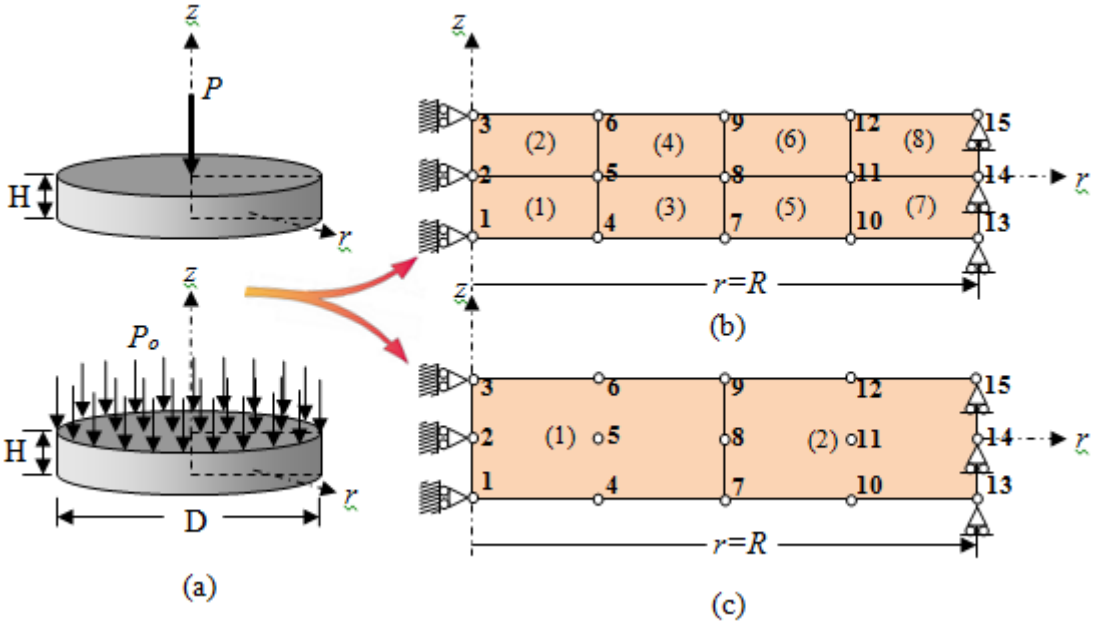

Figure 5: The circular plate (a) loading conditions (b) 8-Ring4 (c) 2-Ring9 element

The exact solution for axial displacement and radial stress of this problem under central point load using Kirchhoff plate theory can be found in [17]. Axial displacements are compared graphically over $a \le r \le b$ with the exact solution in Fig. 6 for the point load at the center of the circular plate. As seen in Fig. 6(a) the axial displacements have the right pattern but the values are under estimated with Ring4. This is a mild case of so-called "shear locking" in which significant amount of element energy is spent in shear [1]. As seen in Fig. 6(a) increasing the number of Ring4 elements reduces the shear locking but the displacement is still under estimated. The analysis is repeated for Ring9 with half the elements: 2, 4 and 8 respectively in radial direction, and only one element in the axial direction. From Fig. 6(b) it can be seen that the transverse or axial displacement is well captured since the element does not suffer from shear locking.

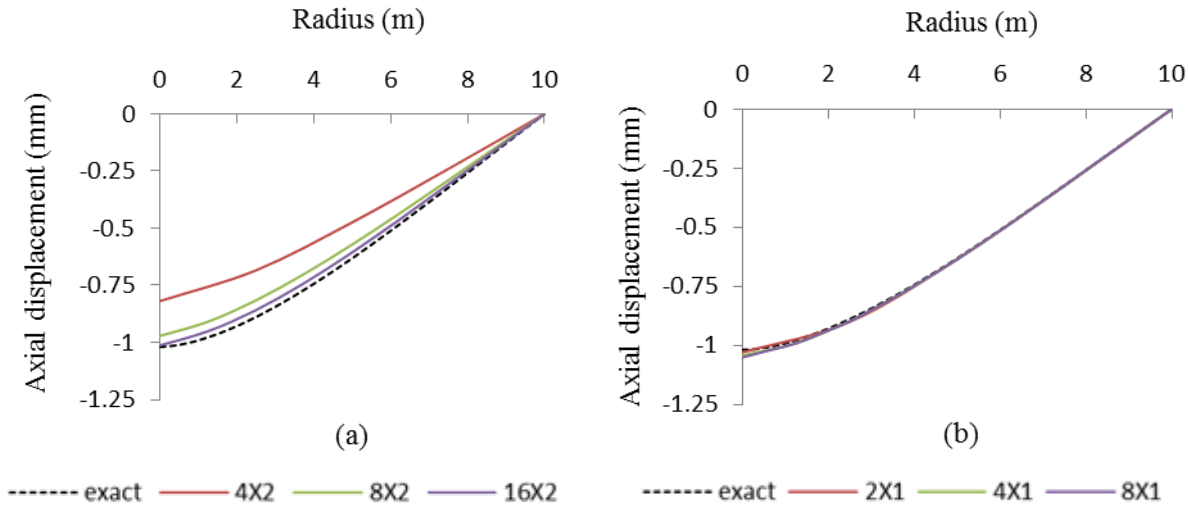

Figure 6: Axial displacements of circular plate with central point load (a) Ring4 (b) Ring9

The shear locking effect is further investigated in detail for various ratios of thickness to diameter of the circular plate. Circular plates under uniformly distributed load with simple supports along the edges are analyzed for different ratios. The convergence rates of the center deflections and radial stresses at the bottom of the plate with increasing number of elements for four different ring elements are shown in Figs. 7 and 8. These are the bilinear 4 node element with full integration Ring4(FI) and selectively reduced integration Ring4(SRI) and the biquadratic 9 node element with full integration Ring9(FI) and selective reduced integration Ring9(SRI). Non-dimensional center displacements and radial stresses are presented in figures using $D^*=EH^3/(12(1-\nu^2))$. The results are compared with the exact solution obtained by Kirchoff thin plate theory.

As shown in Figs. 7 and 8 the rate of convergence of Ring4 (FI) is too slow below a certain limit of thickness to diameter ratio. In Fig. 7(a) it can be easily seen that the required number of elements for an acceptable convergence of element Ring4(FI) to the exact solution is too large for the small ratio of H/D=0.001. Therefore, for the purpose of computational cost and computer capacities it is important to avoid from such locking effects. As can be seen from Figs. 7 and 8 increasing the ratio of thickness to diameter accelerates the convergence rate of the Ring4(FI). However, it is possible to reach an optimal rate of convergence for coarse meshes using selectively reduced integration element Ring4(SRI) in the analysis of even very thin plates as shown in Figs. 7(a) and 8(a). Additionally, it can be realized from Figs. 7 and 8 that the convergence of Ring4(SRI) is uniform with respect to thickness to diameter H/D ratio.

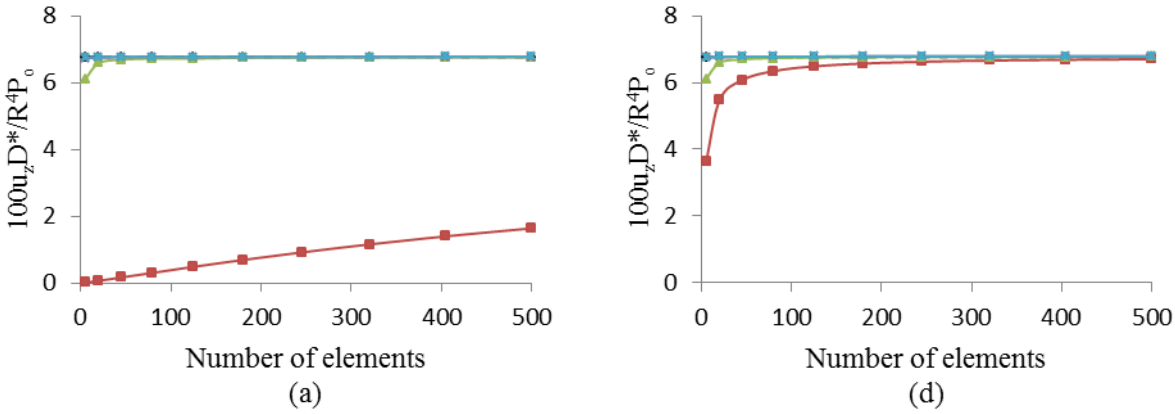

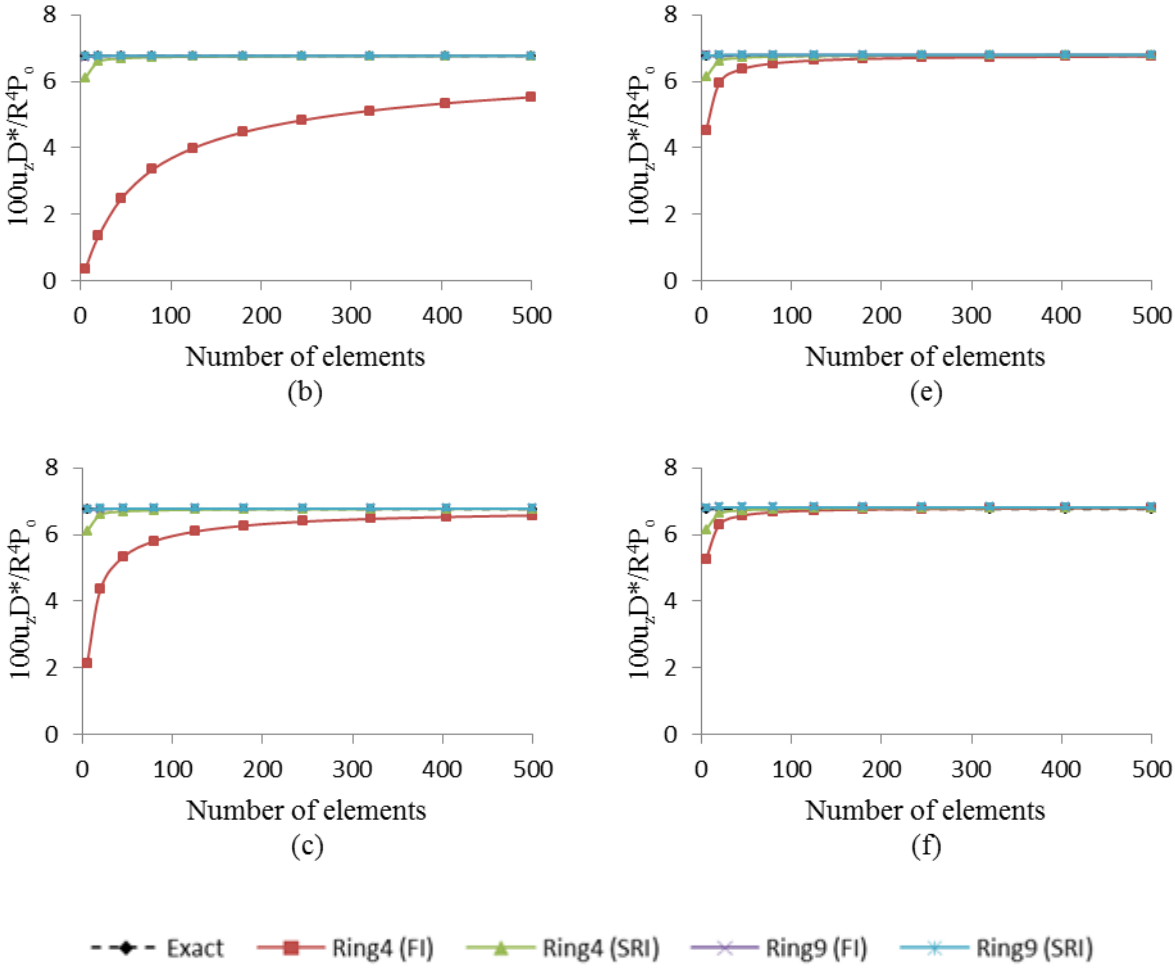

Figure 7: Non-dimensional center displacement versus number of elements for various thickness to diameter ratios (a) H/D=0.001 (b) H/D=0.005 (c) H/D=0.015 (d) H/D=0.025 (e) H/D=0.035 (f) H/D=0.05

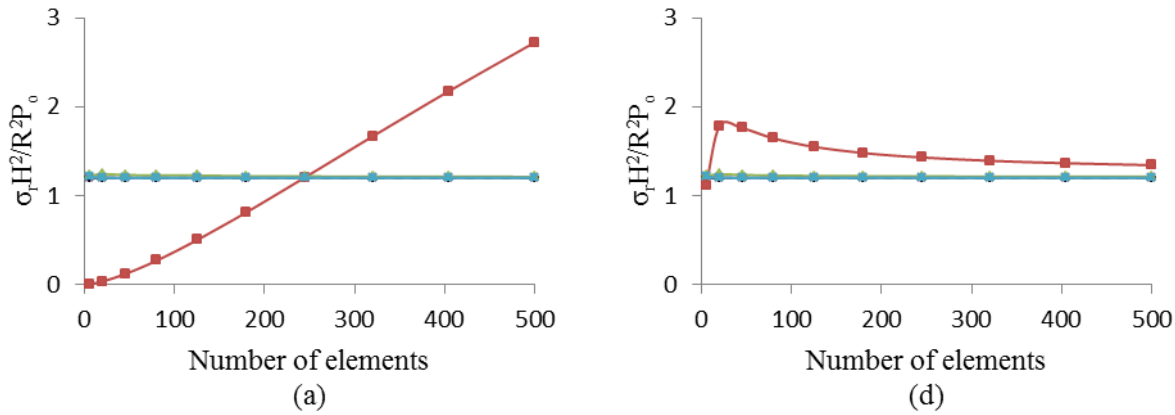

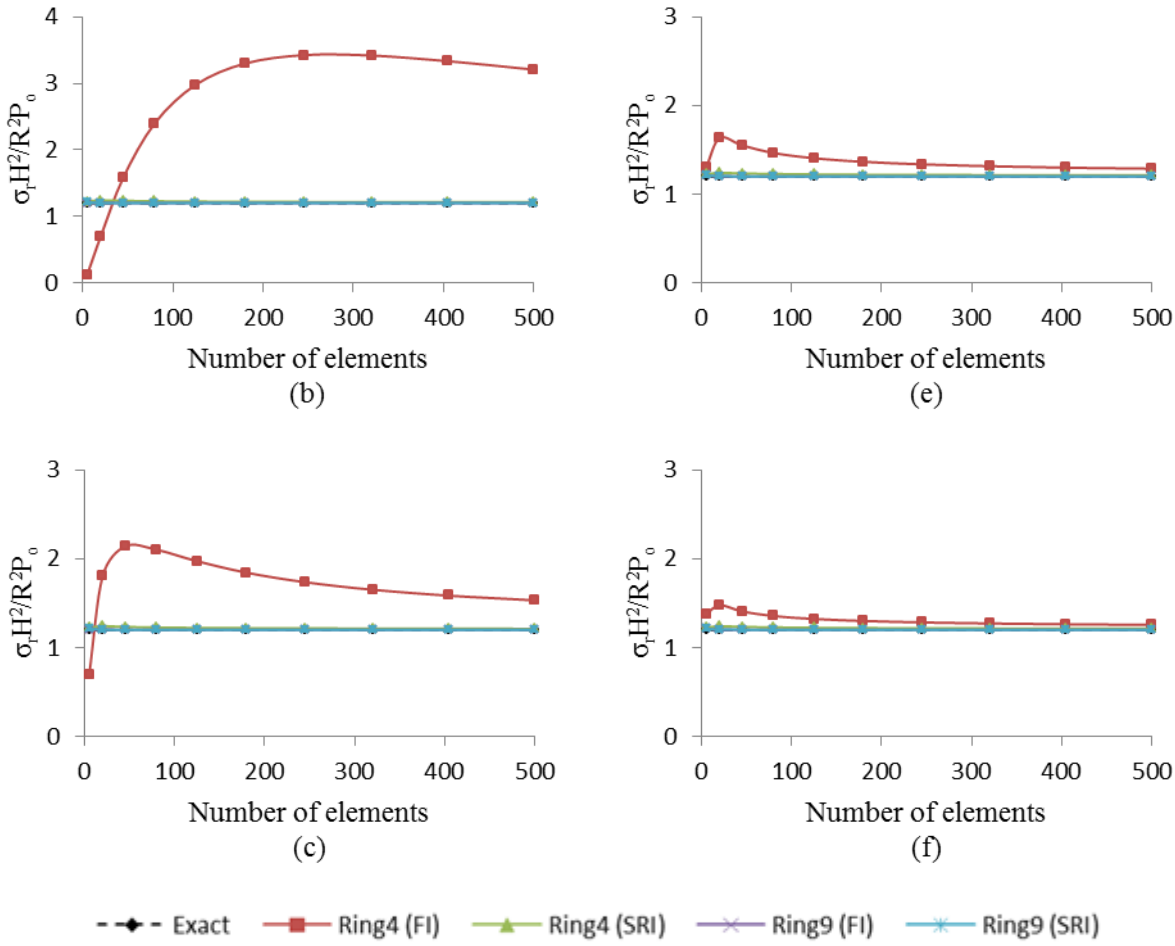

Figure 8: Non-dimensional radial stresses versus number of elements for various thickness to diameter ratios (a) H/D=0.001 (b) H/D=0.005 (c) H/D=0.015 (d) H/D=0.025 (e) H/D=0.035 (f) H/D=0.05

Also, it can be stated that the convergence rate of Ring4(SRI) element is still smaller than that of Ring9(FI) and Ring9(SRI) elements since these are the higher-order elements based on quadratic shape functions. Although Ring9(FI) element shows no signs of shear locking in this problem it is not guaranteed that its performance would be good for different type of loading and boundary conditions. However, its performance can be improved if SRI technique is used for shear strain energies as explained previously. Using Ring9(FI) or Ring9(SRI) in the analysis of circular plate, displacement and radial stresses can be obtained with the same accuracy and rate of convergence for coarse meshes. The rate of convergence of these elements is independent of the thickness to diameter ratio, H/D. In Figs. 9 and 10, dimensionless center displacements and radial stresses are plotted against various thickness to diameter ratios.

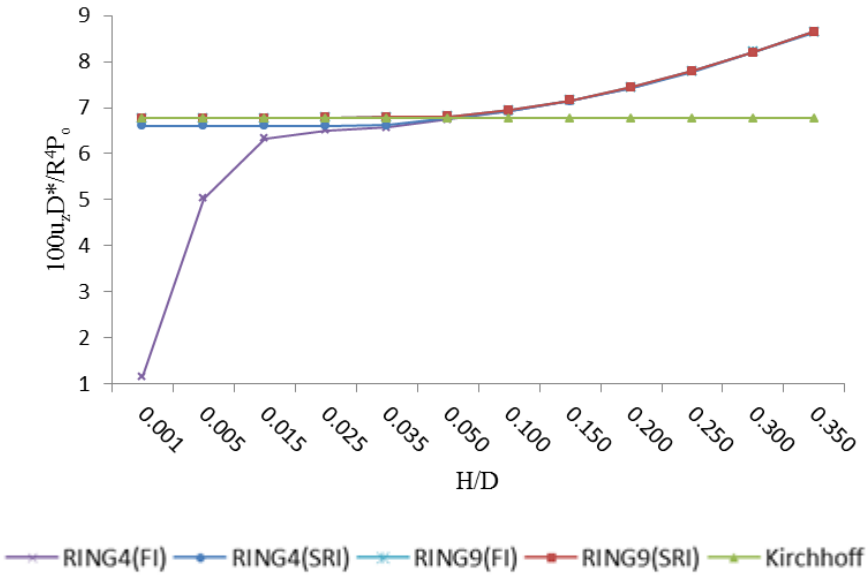

Figure 9: Dimensionless center displacements of simply supported circular plate under uniformly distributed load

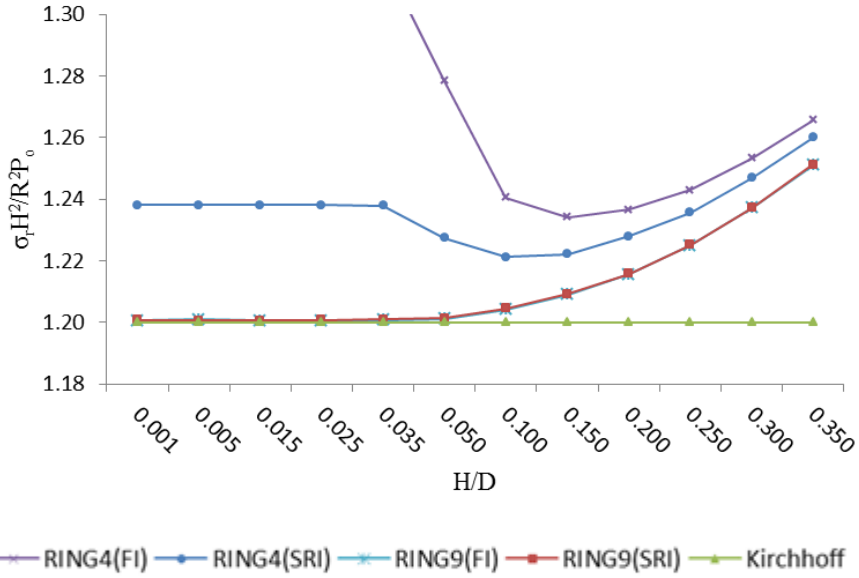

Figure 10: Dimensionless center radial stresses at the bottom surface of the simply supported circular plate under uniformly distributed load

Four types of ring elements are used in the analysis of the circular plate for different thicknesses. It can be seen from Figs. 9 and 10 that all lines intersect or come so close to each other at the ratio of H/D=0.05 and H/D=0.1 for center displacements and radial stresses, respectively. Therefore, it can be stated that shear locking problem disappears above these certain limits for the elements suffering from shear locking. Also it can be observed from Figs. 9 and 10 that below the limit of H/D=0.05 the displacement and stress values of Ring9(FI) and Ring9(SRI) elements coincide with those of Kirchhoff thin plate theory while above these limits the values obtained using these elements move away from the Kirchhoff solutions. This means that results by Kirchhoff thin plate theory deviate as the plate gets thicker since the transverse shear deformations are ignored. Moreover, it can be concluded that Ring4(SRI) can be used as a locking free element although the absolute errors of locking

free elements such as Ring9(FI) and Ring9(SRI) are much smaller due to the order of the shape functions used in the formulations. Table 3 and 4 present the dimensionless values of center displacements and center radial stresses at the bottom of the circular plates respectively for various thickness to diameter ratios or for different thin circular plates (below H/D=0.05) and for thick circular plates (above H/D=0.05) with the given number of elements in axial (n_{ez}) and radial directions (n_{er}).

Table 3. Dimensionless center displacements of simply supported circular plates under uniformly distributed load for various thickness/diameter ratios and integration techniques

H/D	RING4 FI	RING9 FI	RING4 SRI	RING9 SRI	RING4 Mesh (n_{er}xn_{ez})	RING9 Mesh (n_{er}xn_{ez})
	$100u_zD^*/(P_oR^4)$					
0,001	1,1527	6,7674	6,6027	6,7698	40x2	20x1
0,005	5,0230	6,7686	6,6030	6,7702	40x2	20x1
0,015	6,3267	6,7726	6,6063	6,7731	40x2	20x1
0,025	6,5085	6,7805	6,6128	6,7807	40x2	20x3
0,035	6,5703	6,7910	6,6225	6,7911	40x2	20x3
0,050	6,7442	6,8131	6,7686	6,8132	40x4	20x3
0,100	6,9233	6,9426	6,9259	6,9426	40x7	20x6
0,150	7,1460	7,1541	7,1444	7,1541	40x10	20x6
0,200	7,4366	7,4415	7,4334	7,4415	40x12	20x6
0,250	7,7941	7,7956	7,7898	7,7956	40x16	20x7
0,300	8,2039	8,2037	8,1991	8,2037	40x20	20x8
0,350	8,6488	8,6474	8,6434	8,6473	40x24	20x10

Table 4. Dimensionless radial stresses at the bottom of simply supported circular plates under uniformly distributed load for various thickness/diameter ratios and integration techniques

H/D	RING4 FI	RING9 FI	RING4 SRI	RING9 SRI	RING4 Mesh (n_{er}xn_{ez})	RING9 Mesh (n_{er}xn_{ez})
	σ_rH^2/P_oR^2					
0,001	1,7466	1,2006	1,2382	1,2007	40x2	20x1
0,005	3,4882	1,2010	1,2382	1,2007	40x2	20x1
0,015	1,6564	1,2007	1,2381	1,2007	40x2	20x1
0,025	1,3942	1,2007	1,2381	1,2009	40x2	20x3
0,035	1,3183	1,2008	1,2380	1,2010	40x2	20x3
0,050	1,2784	1,2012	1,2274	1,2014	40x4	20x3
0,100	1,2406	1,2042	1,2213	1,2045	40x7	20x6
0,150	1,2342	1,2090	1,2223	1,2092	40x10	20x6
0,200	1,2366	1,2156	1,2280	1,2158	40x12	20x6
0,250	1,2430	1,2251	1,2358	1,2253	40x16	20x7
0,300	1,2532	1,2371	1,2469	1,2372	40x20	20x8
0,350	1,2657	1,2511	1,2600	1,2513	40x24	20x10

5. Conclusions

An investigation is performed to see the effect of volumetric and shear locking effects on the performance of 4 and 8-noded harmonic solid ring finite elements. For this purpose, several benchmark problems such as internally pressurized thick cylinder and circular plate in bending are solved by the coded program in Matlab. The program is capable of solving problems with 4-noded (Ring4) and 9-noded (Ring9) harmonic solid ring elements using full or selectively reduced integration techniques in finite element procedure. The axial displacements and radial stresses are compared with the exact solutions obtained from the literature. Most important conclusions can be drawn from the study are as follows:

- In the case of hollow cylinder problem under axial load, axial torque and lateral load the relative errors compare to analytical solutions are very small for both Ring4 and Ring9 and decrease with the mesh refinement.
- Volumetric locking problem is observed using Ring4 in case of internally pressurized thick cylinder for high values of Poisson's ratio. However, Ring9 does not suffer from this type of locking problem.
- Shear locking problem is observed using Ring4 in the case of plate bending problem. The convergence rate of Ring4 becomes much smaller when the thickness to diameter ratio of the circular plate is decreased but that of Ring9 is not significant.
- While Ring4 (SRI) with selectively reduced integration eliminates the shear locking problem Ring9 (SRI) produces excellent results due to higher order displacement functions in the formulation.
- Results obtained using full integration and selectively reduced integration come very close to each other at the ratio of H/D=0.05 and H/D=0.1 for the center displacements and the radial stresses in the plate bending. That means that above these certain limits shear locking disappears for the circular plate problem.

Acknowledgments

The first author has been supported by TUBITAK (Turkish Scientific and Technological Research Council) with a scholarship which is gratefully acknowledged.

References

[1] Felippa, A.C., IFEM Lecture Notes, Department of Aerospace Engineering Sciences, University of Colorado at Boulder, 2011.
[2] Bell, R.W., Houlsby, G.T. and Burd, H.J., Suitability of three-dimensional finite elements for modelling material incompressibility using exact integration, *Communications in Numer. Methods in Eng*, 9(4), 313-329, 1993.
[3] Oñate, E., Rojek, J., Taylor, R.L., Zienkiewicz, O.C., Finite calculus formulation for incompressible solids using linear triangles and tetrahedral*, Int. J. Numer. Methods in Eng.,* 59(11), 1473-1500, 2004.
[4] Bart V., Volumetric locking in finite elements, Bachelor Final Project, Eindhoven University of Technology, Department of Mechanical Engineering, 2008.
[5] Korhan, Ö. and Ayse, T.D., Elastik zemine oturan kalın plaklar için kayma kilitlenmesiz bir sonlu eleman modeli. *İMO Teknik Dergi*, 346, 5341-5358, 2011.
[6] Pugh, E.D.L., Hinton, E. And Zienkiewichz, O.C., A study of quadrilateral plate bending

elements with reduced integration*, Int. J. Numer. Methods in Eng.*, 12(7), 1059-1079, 2005.
[7] Alves de Sousa, R.J., Natal Jorge, R.M., Fontes Valente, R.A. and Cesar de Sa, J.M.A., A new volumetric and shear locking-free 3D enhanced strain element, *Eng.Computations*, 20(7), 896-925, 2003.
[8] Malkus, D.S., Hughes, T.J.R., Mixed finite element methods - reduced and selective integration techniques: a unification of concepts, *Comp. Methods in Appl. Mech. Eng.* 15(1), 63-81, 1978.
[9] Lee, P.S. and Bathe, K.J., On the asymptotic behavior of shell structures and the evaluation of finite element solutions, *Comp. and Struct.*, 80, 235-255, 2002.
[10] Cook, R.,D., Malkus, D.,S. and Plesha, M.,E., Concepts and Applications of Finite Element Analysis, 3rd Edition, Wiley & Sons, USA, 1989.
[11] Ali, İ.Karakaş, Static and Dynamic Analyses of Axisymmetric Structures Using Harmonic Solid Ring Finite Element Modeling, Master dissertation. Karadeniz Technical University, Turkey, 2012.
[12] Benasciutti, D., De Bona, F. and Munteanu, M.Gh., Numerical analysis-theory and application, In: Awrejcewicz J. editor, University of Udine, 2011.
[13] Bathe, K.J., Finite Element Procedures, Prentice-Hall, USA, 1996.
[14] Bhatti MA. Advanced Topics in Finite Element Analysis of Structures: with Mathematica and Matlab Computations, USA: John Wiley&Sons, 2006.
[15] Halil, K., Spectral Analysis Program of Structures: SAPOS User Manual, Delft University of Technology, Netherlands, 79-90, 2009.
[16] Timoshenko, S. and Goodier, J.N., Theory of Elasticity, McGraw-Hill, New York,1951.
[17] Ugural, A.C., Stresses in Plates and Shells, McGraw-Hill, USA, 1981.